 CMES, vol.95, no.5, pp.369-390, 2013

Simulation of Free Surface Flow with a Revolving Moving Boundary for Screw Extrusion Using Smoothed Particle Hydrodynamics

T.W. Dong[1], H.S. Liu[1], S.L. Jiang[2], L.Gu[1], Q.W. Xiao[1], Z. Yu[1], X.F. Liu[3]

Abstract: In this paper, we present a free surface flow model with a forced revolving moving boundary for partially filled screw extrusion. The incompressible smoothed particle hydrodynamics (ISPH) is used to simulate this complex flow. A set of organic glass experimental device for this partially filled fluid is manufactured. SPH results are satisfactorily compared with experiment results. The computed free surfaces are in good agreement with the free surfaces obtained from the experiment. Further analysis shows that with the increase of the speed, the average velocity of fluid increases, the effect of centrifugal force begin to show up, the maximum pressure increase. It has been proved that the ISPH method is effective in simulating the partially filled flow problem for screw extrusion. This lays a foundation for future research on more complex flows in screw extrusion.

Keywords: Incompressible smoothed particle hydrodynamics, forced revolving moving boundary, free surface flow, screw extrusion.

1 Introduction

Forced moving boundary problem is frequently encountered in many industrial areas such as stirring, forced conveying, and wave making. For example, in the field of polymer processing, single-screw extrusion simulation and twin-screw extrusion simulation are a typical forced moving boundary problem. The traditional simulation method such as the finite volume (FV) and finite element method (FEM) are often used to simulate the screw extrusion. Khalifeh and Clermont (2005) use FV to simulate non-isothermal three-dimensional flows in a single-screw extruder.

[1] School of Physics and Electronic information, Shangrao Normal University, Shangrao 334001, China.
Email: tianwendong@live.cn
[2] School of Information Engineering, Nanchang University, Nanchang 330031, China.
[3] College of Chemistry and Chemical Engineering, Hunan University, Changsha, 410000, China.

A remeshing technique in FEM is applied to calculate flow characteristics in twin and multi-screw extruder [Zhu, Yuan and Wang (2009)]. However, the remeshing technique is very time-consuming. The commercial software POLYFLOW is used to model 3D flow in twin-screw extruder [Barrera, Vega and Mart'ınez-Salazar (2008)]. In this software a special technique called the mesh superposition technique (MST) is used to treat moving boundary, avoiding using the complex remeshing technique. MST requires data interpolation between the corresponding superposed meshes (the barrel and the screw) at each time-step; therefore, error will inevitably be caused.

Moreover, in order to simplify calculation, the extruder channel is supposed to be fully filled in almost all of the researches so far, but actually it is partially filled in many zones, especially in twin-screw extrusion. However, neither the remeshing technique nor the MST technique can treat this partially filled flow with a forced revolving moving boundary. So far, only there are a few reports on visualization extrusion experimental research on this complex flow rather than simulation [Graaf, Woldrignh, and Janssen (1999)].

On the other hand, the meshless methods which avoid any mesh distortion have now been developed to compute both fluid and solid dynamics problems. So far, there are more than twenty different kinds of meshless methods, see the review written by Belytschko, Nguyen and co-workers [Belytschko, Krongauz, Organ, Fleming and Krysl (1996) and Nguyen, Rabczuk, Bordas and Duflot (2008)]. In the simulation of complex flows (usually with a moving boundary or a free surface), the meshless methods have shown great advantages over the traditional simulation methods. For example, Monaghan (1994) used the smoothed particle hydrodynamics (SPH) to simulate incompressible free surface flows. Avila and Atluri (2009) employed the meshless local Petrov Galerkin (MLPG) method to simulate a non-steady flow with a moving boundary induced by an undulating body A novel MLPG mixed finite-volume method was presented by Avila Han, and Atluri (2011) to compute a complex Stokes vortex mixing flow Kakuda, Obara, Toyotani, Meguro, and Furuichi (2012) used the moving particle semi-implicit (MPS) method to solve incompressible viscous fluid flow involving free surfaces and gravity. Kakuda, Nagashima and coworkers (2012) also introduced their acceleration computation for MPS on GPU (Graphics Processing Units) using CUDA (Compute Unified Device Architecture) Kosec and Sarler (2008) applied the mesh-free local radial basis function collocation method (LRBFCM) to solve the coupled heat transfer and fluid flow problems in Darcy porous media. Among these methods, the SPH is the earliest one introduced by Lucy (1977), Gingold and Monaghan (1977) in a study of astrophysics. For its excellent adaptive nature, SPH perform excellently in dealing with problems such as a moving boundary, large deformation and free surface flow

and has been widely applied in industrial fields, for example, Prakash, Cleary and Grandfield (2009) used SPH to track the free surface flow in the metal casting and predict oxide formation; Moulinec, Issa, Marongiu and Violeau (2008) applied a parallel SPH code to a 3-D dam breaking flow impinging on an obstacle; Campbell, Vignjevic, Patel and Milisavljevic (2009) used a coupled SPH-FEM approach to predict the interaction of large ocean waves with ships.

In order to compute the incompressible flows, Monaghan (1994) presented an equation of state to calculate the pressure for the standard SPH (also named weakly compressed SPH, WCSPH). However, this method has one defect that a small density fluctuation may results in large pressure oscillation. An alternative method is incompressible SPH (ISPH) [Cummins and Rudman (1999)] [Shao and Lo (2003)] [Lee, Moulinec, Xu, Violeau, Laurence and Stansby (2008)] [Xu, Stansby and Laurence (2009)], in which the pressure is implicitly obtained by solving a pressure Poisson equation. The idea of ISPH comes from Chorin's (1968) prediction-correction projection method. Both SPH methods have been used intensively. Lee, Moulinec, Xu, Violeau, Laurence and Stansby (2008) pointed that ISPH yields smoother velocity and pressure results than WCSPH. Recently, Rafiee, Cummins, Rudman and Thiagarajan (2012) also reported that WCSPH strongly overestimated the impact pressure in simulating energetic free-surface flows. The stability and accuracy of ISPH have been intensively studied by Xu, Stansby and Laurence (2009). A moving-least-squares (MLS) method is used to correct the density in WCSPH [Colagrossi and Landrini (2003)] [Delorme, Colagrossi, Souto-Iglesias, amora-Rodriguez, and Botia-Vera (2009)]. Hughes and Graham (2010) compared both methods shows that the MLS corrected WCSPH performed as well as ISPH. In this paper, only ISPH is used.

The purpose of this paper is to prove the effectiveness of the ISPH method in simulating the partially filled flow problem for screw extrusion thus lay a foundation for future research on more complex flows in real screw extrusion. To facilitate the calculation, the calculation model presented is simplified The governing equations and detailed numerical schemes for ISPH are introduced in Section 2. The model of partially filled flow problem for screw extrusion is presented in Section 3. In Sections 4, the experiment background is introduced. In Section 5, the boundary condition treatment of the model is introduced. In Section 6, the computed results and the experiment data are compared and analyzed. The conclusions are presented in Section 7.

2 Theoretical background

2.1 Governing equations

The governing equations are the mass and momentum conservation equations, which are written in Lagrangian

$$\frac{D\rho}{Dt} = -\rho\nabla\cdot\boldsymbol{v} \tag{1}$$

$$\frac{D\boldsymbol{v}}{Dt} = -\frac{1}{\rho}\nabla p + \frac{1}{\rho}\nabla\cdot\boldsymbol{\tau} + \boldsymbol{F} \tag{2}$$

where $\boldsymbol{\tau} = 2\mu\varepsilon - \frac{2}{3}\mu(\nabla\cdot\boldsymbol{v})I, \quad \varepsilon = \frac{1}{2}[\nabla v + (\nabla\boldsymbol{v})^T]$.

2.2 Incompressible SPH algorithm

The incompressible SPH is a prediction-correction projection algorithm [Cummins and Rudman (1999)]. In the prediction step, momentum conservation equation is explicitly integrated without enforcing incompressibility. Then a pressure Poisson equation is deduced by combining the pressure term and the incompressibility. In the correction step, solving the Poisson equation and the pressure will be used to update the particle's velocity and position. There are various choices for enforcing incompressibility: a divergence-free velocity field, density invariance and their combination [Xu, Stansby and Laurence (2009)]. The divergence-free velocity field and density invariance have been tested in calculating the model presented in this paper and the former has been proven to be more effective and accurate.

An intermediate velocity v^* is obtained through Eq.3, in which only viscosity force and external force are considered.

$$\boldsymbol{v}^* = \boldsymbol{v}^n + \left(\boldsymbol{F} + \frac{1}{\rho}\nabla\cdot\boldsymbol{\tau}\right)\Delta t \tag{3}$$

Particle positions r^* don't advance:

$$\boldsymbol{r}^* = \boldsymbol{r}^n \tag{4}$$

Solving the pressure Poisson Eq.5, the pressure at time n+1 can be obtained.

$$\nabla\cdot\left(\frac{1}{\rho}\nabla p^{n+1}\right) = \frac{\nabla\cdot\boldsymbol{v}^*}{\Delta t} \tag{5}$$

Finally, the velocity at time n+1 $\boldsymbol{v}^{n+1}$ is calculated as shown in Eq.6. The particle position r^{n+1} is updated using a second-order time marching scheme.

$$\boldsymbol{v}^{n+1} = \boldsymbol{v}^n - \frac{\Delta t}{\rho}\nabla p^{n+1} \tag{6}$$

$$\boldsymbol{r}^{n+1} = \boldsymbol{r}^n + \Delta t \frac{\boldsymbol{v}^{n+1} + \boldsymbol{v}^n}{2} \tag{7}$$

2.3 Approximations by SPH and Formulations discretization

In SPH, the problem domain is discretized into a set of particles. Each particle carries a mass m, a density ρ, a pressure p and other properties, depending on the problem. The core idea of SPH is that the field variables can be approximated by interpolation over the particles within the support domain, as shown in Eq.8:

$$f(\boldsymbol{r}_i) = \sum_{j=1}^{N} f(\boldsymbol{r}_j) W(\boldsymbol{r}_i - \boldsymbol{r}_j, h) \frac{m_j}{\rho_j} \tag{8}$$

where $f(r_j)$, m_j, and ρ_j are the field value, mass, and density of particle j. W=kernel function and h=smoothing distance. Vector r_i and r_j= position of particle i and j. W is usually written in the form of $W(r_i - r_j, h)$. Throughout this paper, the cubic spline kernel suggested by Shao and Lo (2003) is used.

The gradient term of $f$can be written as:

$$\nabla f(\boldsymbol{r}_i) \cong \sum_{j=1}^{N} \frac{m_j}{\rho_j} f(\boldsymbol{r}_j) \nabla_i W_{\mathrm{ij}} \tag{9}$$

where the $\nabla_i W_{ij}$ denotes the gradient of the kernel. However, Eq.9 is rarely directly used. Usually a symmetric or an asymmetric form of gradient term is used instead [Monaghan (1992)]. The equations in [Lee, Moulinec, Xu, Violeau, Laurence and Stansby (2008)] for the gradient of pressure and the divergence of velocity are applied in this paper:

$$\left(\frac{1}{\rho}\nabla p\right)_i = \sum_{j=1}^{N} m_j \left(\frac{p_i}{\rho_i^2} + \frac{p_j}{\rho_j^2}\right) \nabla_i W_{ij} \tag{10}$$

$$\nabla \cdot \boldsymbol{v}_i = -\frac{1}{\rho_i} \sum_{j=1}^{N} m_j (\boldsymbol{v}_i - \boldsymbol{v}_j) \cdot \nabla_i W_{ij} \tag{11}$$

The viscous term and Laplacian operators are usually discretized by a method combining a finite difference approach and SPH formalism. The viscous term is identical to the one suggested by Morris (1997):

$$\left\{\left(\frac{1}{\rho}\nabla \cdot \mu \nabla\right)\boldsymbol{v}\right\}_i = \sum_{j=1}^{N} \frac{m_j(\mu_i + \mu_j)\boldsymbol{r}_{ij} \cdot \nabla_i W_{ij}}{\rho_i \rho_j (\left|\boldsymbol{r}_{ij}\right|^2 + 0.01h^2)} \boldsymbol{v}_{ij} \tag{12}$$

where μ is dynamic viscosity coefficient; $\boldsymbol{r}_{ij} = \boldsymbol{r}_i - \boldsymbol{r}_j$; $\boldsymbol{v}_i$ is the velocity of particle i, $\boldsymbol{v}_{ij} = \boldsymbol{v}_i - \boldsymbol{v}_j$. The Laplacian operator in the Poisson equation suggested by Shao and Lo (2003) is used here.

$$\nabla \cdot \left(\frac{1}{\rho} \nabla p \right)_i = \sum_{j=1}^{N} m_j \frac{8}{(\rho_i + \rho_j)^2} \frac{p_{ij} \boldsymbol{r}_{ij} \cdot \nabla_i W_{ij}}{\left| \boldsymbol{r}_{ij} \right|^2 + 0.01h^2} \tag{13}$$

The coefficient matrix of the linear system is symmetric and positive definite, and can be solved efficiently by BI-CGSTAB [Van Der Vorst, H.A (1992)] iterative method with a Jacobi pre-conditioner. During the simulation, the convergence criterion is set as 1.0×10^{-3} for the normalized residual.

2.4 Time stepping

The time step Δt is governed by two stability constraint: the CFL condition and the mass force conditions.

$$\Delta t = \min \left(0.25 \frac{h}{v_{\max}}, 0.25 \min_i \left(\frac{h}{f_i} \right)^{1/2} \right) \tag{14}$$

where f_i is external force per unit mass, $v_{\max}$ is the maximum fluid velocity.

2.5 Methods for improving stability

In SPH, when negative pressure appears in some region of the computational domain, the tensile instability may occur, resulting in a local cluster of particles. To overcome this difficulty, researchers have proposed various measures [Hu and Adams (2009)] [Monaghan (2000)]. In this paper, the method presented by Hu and Adams (2009) is used, in which a reference pressure is set as the magnitude of the minimum negative pressure.

3 Model of partially filled flow problem for screw extrusion

A two-dimensional (2D) partially filled forced revolving moving boundary problem model for screw extrusion is shown in Fig.1. An inner fan-shaped small tank revolves uniformly in a clockwise direction about the center of a stationary barrel. The fluid to be processed is sealed in the small tank by the barrel, and the tank is only half filled. It should be pointed out that the purpose of presenting this model is to conform the effectiveness of SPH in calculating a complex free surface flow with a forced revolving moving boundary. Therefore to facilitate the calculation, the size of the model is not completely in conformity with the real screw extruder.

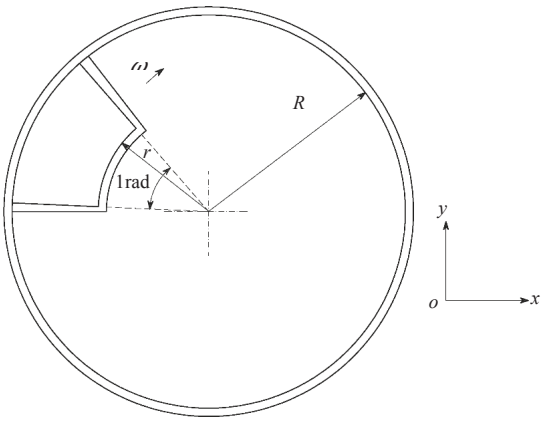

Figure 1: Forced revolving moving boundary model.

Instead of molten polymer, glycerol is used as the fluid. The simulation results will be compared with the experimental results in section 6. The inside radius of the barrel R=0.1m, the depth of the fan-shaped tank Rr=0.05m, the angle of the fan-shaped tank is 1rad, angular velocity of the tank ω=1.5rad/s, the fluid's density $\rho = 1.26 \times 10^3 \text{kg/m}^3$, Re=9.7, such that dynamic viscosity ν=1/Re. No-slip boundary condition and homogeneous Neumann pressure boundary condition, i.e., $\partial p/\partial n$=0 are applied. The initial velocity and pressure of all particles are set to zero.

4 Experiment background

To verify the simulation results, a set of plexiglass glass fluid experimental device is designed. As shown in Fig.2, the core part of the device is a plexiglass component which is mainly composed of a plexiglass cylinder and an open fan-shaped tank. There is a flange on each end of the cylinder, and two end-plates are fixed on the flange. The tank is connected to the shaft through a key, and the shaft is driven by an AC motor with a velocity control unit (i.e. governor). The sizes of this device are the same with the sizes of the computing model presented in section 4. Because the thickness of the tank (0.01m) is very small, it can be treated as a 2D flow that is in agreement with the calculation model. The glycerol is sealed in the fan-shaped tank by the barrel. That one layer of flexible material is placed between the tank and the cylinder can not only avoid the leakage of glycerol, but also ensure the tank revolve stably. There is a hole separately in one end-plate and one side of the tank, and glycerol can be injected to the tank through these holes. To conveniently

observe the flow, the glycerol is dyed. In addition, a digital camera is used to record the free surface flow of the glycerol. Finally, the video will be edited into photos for analysis.

Figure 2: Photograph of the experiment platform.

5 Boundary conditions treatment

5.1 Wall boundary

Generally, there are three boundary treatment methods for SPH method: repulsive force boundary [Monaghan (1994)] [Monaghan and Kos (1999)], mirror boundary [Cummins and Rudman (1999)] and dummy boundary [Lee, Moulinec, Xu, Violeau, Laurence and Stansby (2008)]. The repulsive force boundary method was first developed by Monaghan (1994), similar to those in molecular dynamics. The particles on wall could exert large repulsive force on the inner fluid particles to prevent them from crossing the wall. However, this method has a defect that the particles tend to "wobble" when moving parallel to the wall. The mirror and dummy boundary method is applied more widely. Lee, Moulinec, Xu, Violeau, Laurence and Stansby (2008) pointed out that the mirror boundary isn't fit for curved boundary or corner. All three methods have been tried in our computation and the conclusions are almost identical with the researches before. Thus, only the dummy boundary is introduced in this paper.

Besides the boundary conditions, the initial particles configurations are also very important for SPH. Monaghan (2006) pointed out that the initial configuration particles placed on rings provide the most accurate solution. As shown in Fig.3, the particles are initially arranged at equal intervals on the concentric rings that are also at equal intervals. Boundary is constructed by the wall particles and dummy particles. The boundary consists of one layer of wall particles and four layers of dummy particles placed outside the wall in the normal direction. In order to clearly represent the boundary and inner particles distribution, the particles around the corner are locally enlarged, as shown in Fig.4. The squares denote the boundary particles, and the circles denote the inner particles. In order to avoid the fluid particles penetrating the boundary, the interval between two neighbor wall particles are one half of the dummy particles'. The interval between two fluid particles r=0.02. There are 3384 particles including 1825 inner particles and 1559 boundary particles in total. Homogeneous Neumann conditions for pressure are applied, i.e. a dummy particle carries identical pressure value as the wall particle in its normal direction. For the moving boundary, the boundary particles' position and velocity is reset according to the tank's new position each time step. The velocity of the boundary particles on the barrel (i.e. the cylinder) is set to zero throughout the simulating.

5.2 Free surface

As shown in Fig.3, the tank is half-filled with glycerol. Since no fluid particle exists outside the free surface, the density of the surface particles calculated using Eq.8 drops significantly. Shao (2012) suggested that if the density drop of a particle is

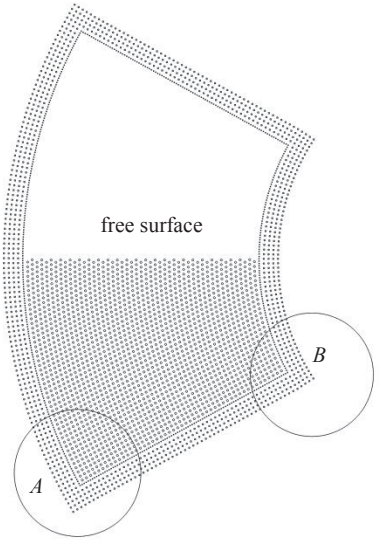

Figure 3: Particle initial configurations

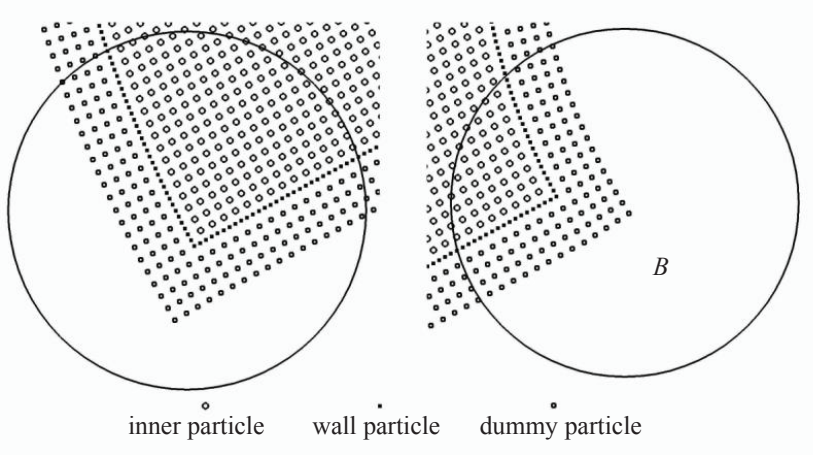

Figure 4: Enlarged area A and B

below 5% of the reference value, it is regarded as being on the free surface. A Dirichlet boundary condition of zero pressure is given to this particle.

6 Results and discussion

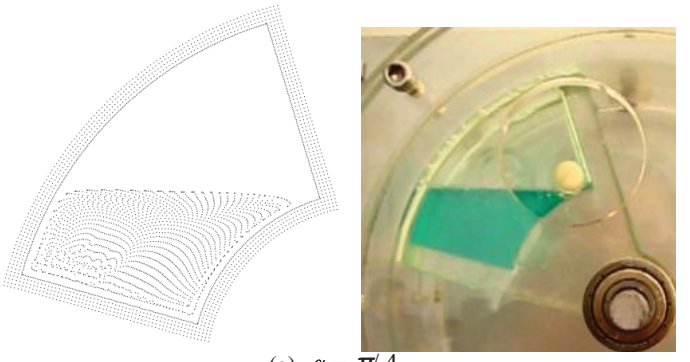

(a) $\alpha = \pi/4$

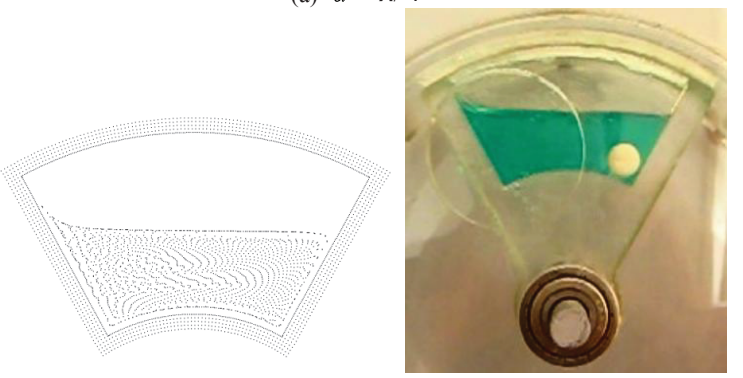

(b) $\alpha = \pi/2$

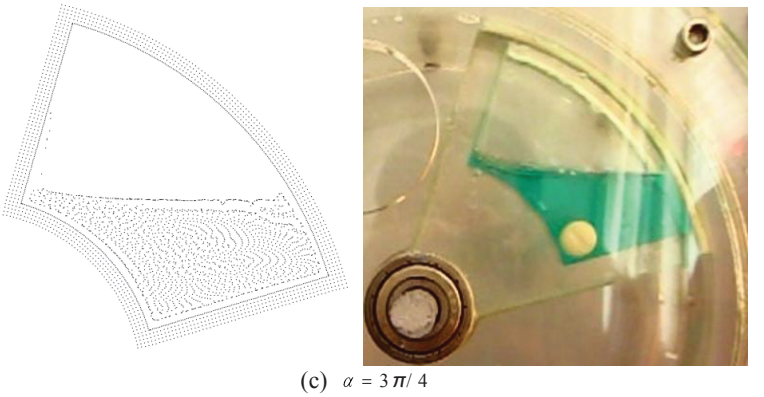

(c) $\alpha = 3\pi/4$

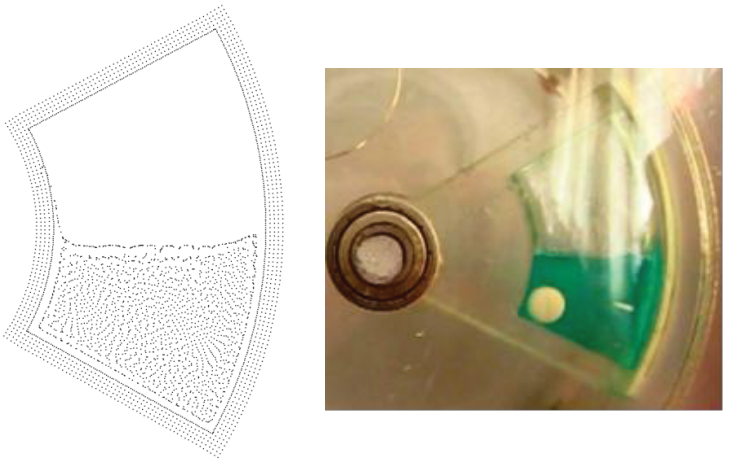

(d) $\alpha = \pi$

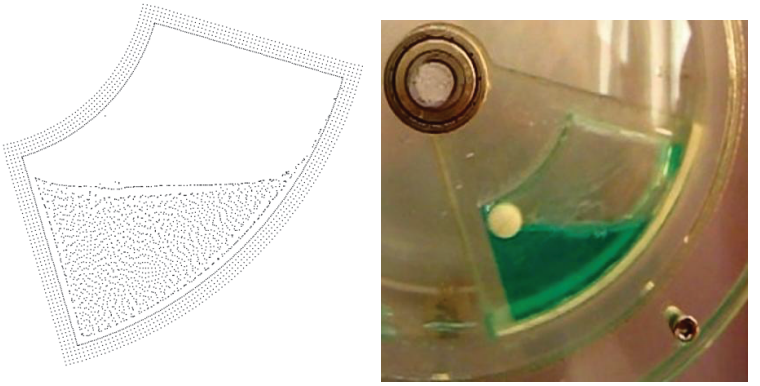

(e) $\alpha = 5\pi/4$

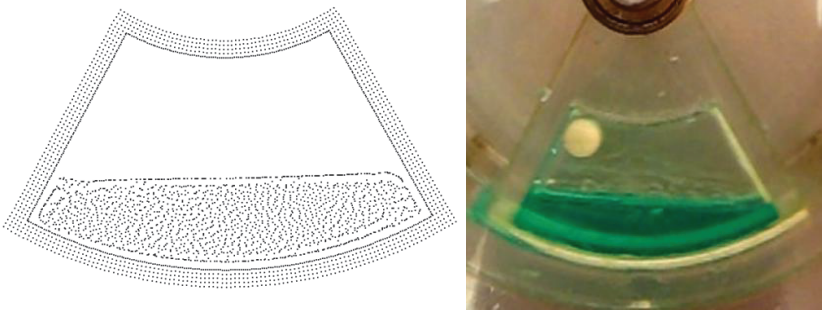

(f) $\alpha = 3\pi/2$

(g) $\alpha = 7\pi/4$

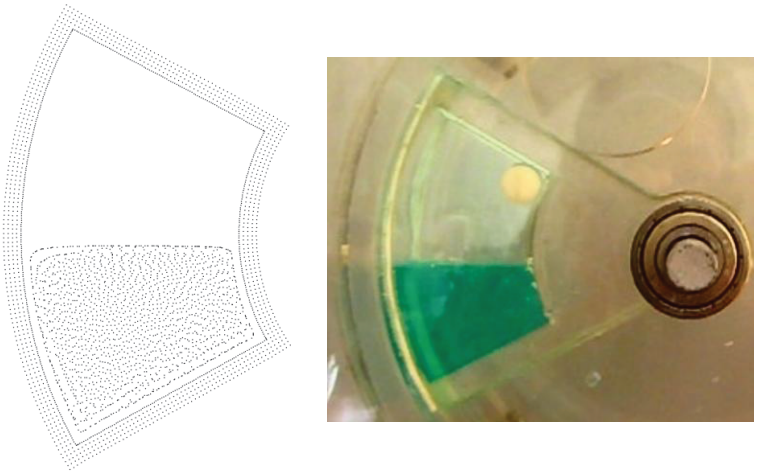

(h) $\alpha = 2\pi$

Figure 5: Results calculated by ISPH against the experiment results ($\omega = 0.5$ rad/s)

Fig.5 and Fig.6 separately shows the results calculated by ISPH against the experiment results at two different angular velocities of 0.5rad/s and 2.5rad/s. αrepresents the rotation angle at $\pi/4$intervals in one full circle. Both of them are consistent with the experimental results. In the case of a lower angular velocity ($\omega = 0.5$ rad/s), the free surface calculated almost appears as a horizontal line; when at a higher angular velocity ($\omega = 2.5$ rad/s), the fluid pushed by the wall more intensely and the free surface shows a curve under the action of the tank and barrel. One "clearance" appears between the fluid particles and wall. It is due to the double numbers of wall particles exert more pressure on the fluid particles. There are a few splashing fluid

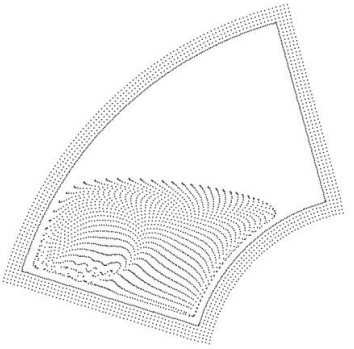

(a) $\alpha = \pi/4$

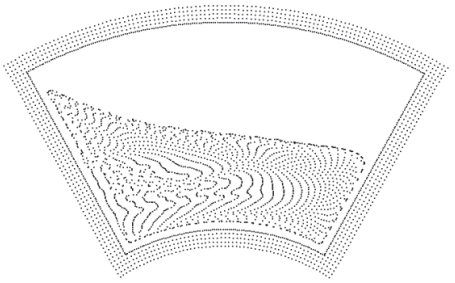

(b) $\alpha = \pi/2$

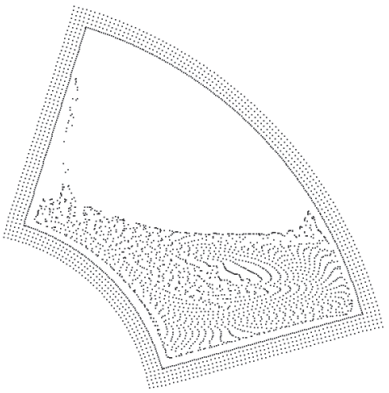

(c) $\alpha = 3\pi/4$

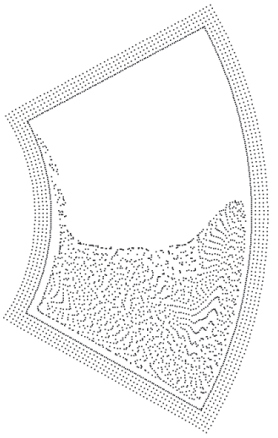

(d) $\alpha = \pi$

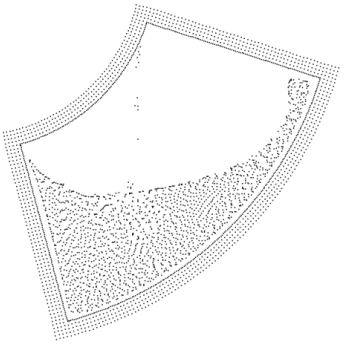

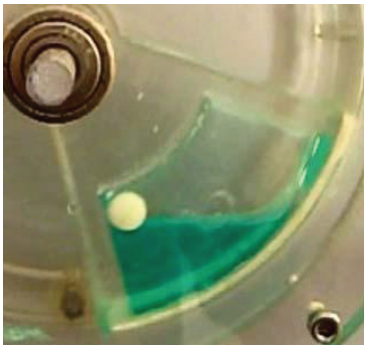

(e) $\alpha = 5\pi/4$

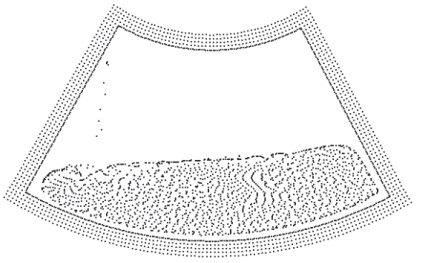

(f) $\alpha = 3\pi/2$

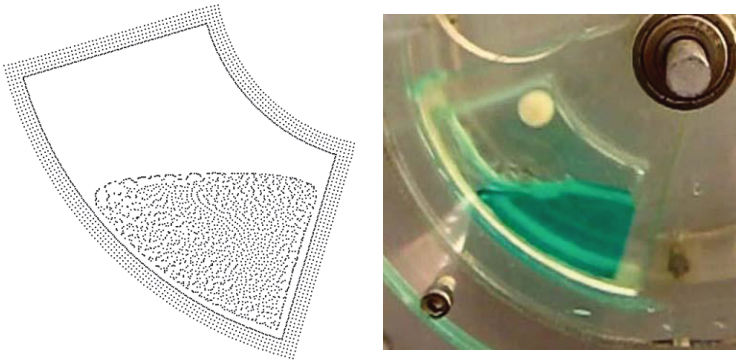

(g) $\alpha = 7\pi/4$

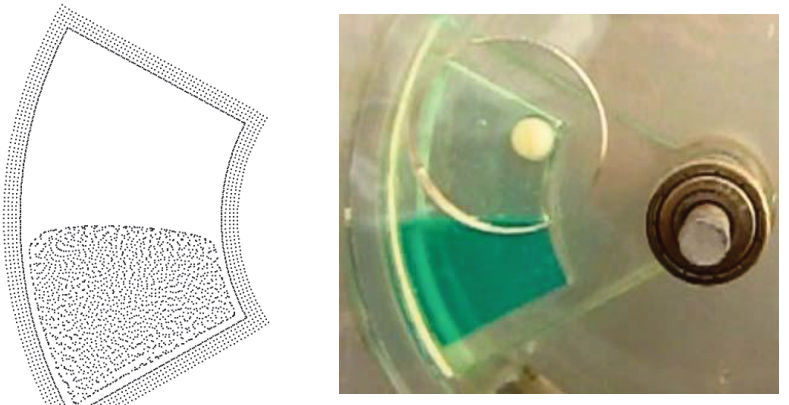

(h) $\alpha = 2\pi$

Figure 6: Results calculated by ISPH against the experiment results ($\omega = 2.5$ rad/s)

particles in Fig.5c, Fig.5d, Fig.5e, Fig.6c, Fig.6d, Fig.6e and Fig.6f. It is because that the fluid particles near the border may adhere to the wall. In Fig.6a and Fig.6b, the fluid is mainly push forward by the left side wall. In Fig.6c, Fig.6d and Fig.6e, the barrel shears the fluid strongly, thus, the free surface shows a completely different form from that in Fig.5c, Fig.5d and Fig.5e. The free surface on the barrel side has a small convex tip in both the calculated results and the experiment results.

Fig.7 and Fig.8 respectively shows the velocity distribution at $\omega = 0.5$ rad/s and $\omega = 2.5$ rad/s. Comparing the reference velocity in Fig.7 and Fig.8, it can be found that the average velocity of fluid increases with the increasing of the revolving speed of the screw. When $\alpha = 3\pi/2$, the screw rotates to the bottom of the barrel, the particles in the bottom are sheared intensely by the inner wall of the barrel,

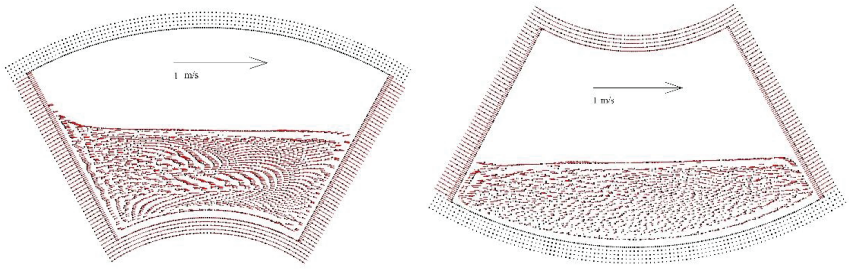

(a) $\alpha = \pi/2$ (b) $\alpha = 3\pi/2$

Figure 7: Velocity distribution for $\alpha = \pi/2$ and $\alpha = 3\pi/2$ with $\omega = 0.5$ rad/s

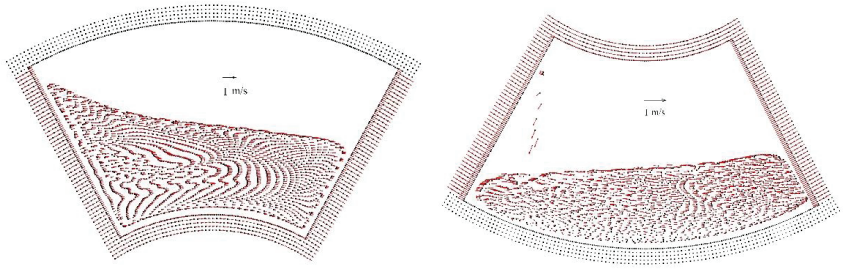

(a) $\alpha = \pi/2$ (b) $\alpha = 3\pi/2$

Figure 8: Velocity distribution for $\alpha = \pi/2$ and $\alpha = 3\pi/2$ at $\omega = 2.5$ rad/s

thus the velocity of these particles is extremely low. From Fig.7b and Fig.8b, it is very clear that the velocity of the particles near the right side wall is comparatively higher than other particles, especially for the higher angular velocity case.

Fig.9 shows the comparison of the particles' distribution considering centrifugal force or not at $\omega = 0.5$ rad/s and $\omega = 2.5$ rad/s at the top of the barrel. Each picture is locally enlarged. It can be observed that at a higher speed, the effect of centrifugal force is more apparent and at a lower speed, the effect of centrifugal force can be negligible.

Fig.10 and Fig.11 separately shows the pressure distribution at $\omega = 0.5$ rad/s and $\omega = 2.5$ rad/s in two different positions. It shows that the range of the pressure becomes wider with a higher angular velocity. The range of the pressure become wider for $\alpha = 3\pi/2$ than $\alpha = \pi/2$. It is because the bottom particles are intensely sheared by the inner wall of barrel when the screw rotates to the bottom of the barrel. The range of the pressure in Fig.11b is wider than in Fig.10b, it is caused

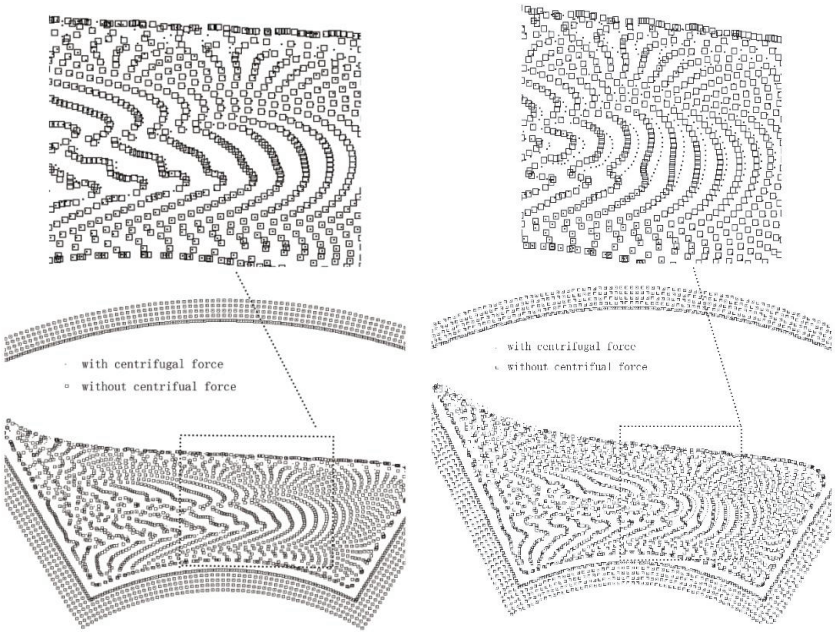

(a) $\omega = 0.5$ rad/s (b) $\omega = 2.5$ rad/s

Figure 9: Particles distribution at $\omega = 0.5$ rad/sand $\omega = 2.5$ rad/s for $\alpha = \pi/2$

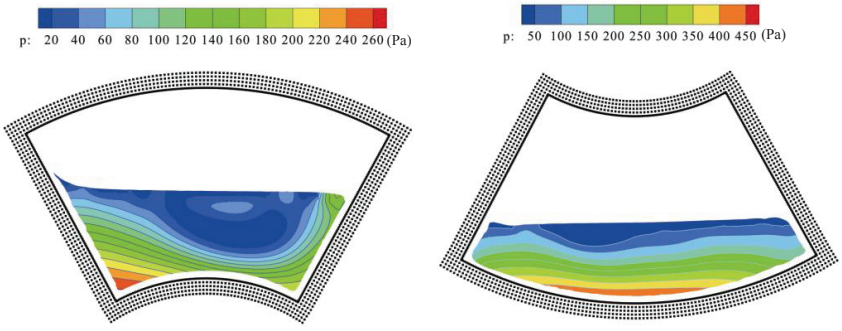

(a) $\alpha = \pi/2$ (b) $\alpha = 3\pi/2$

Figure 10: Pressure distribution for $\alpha = \pi/2$ and $\alpha = 3\pi/2$ at $\omega = 0.5$ rad/s

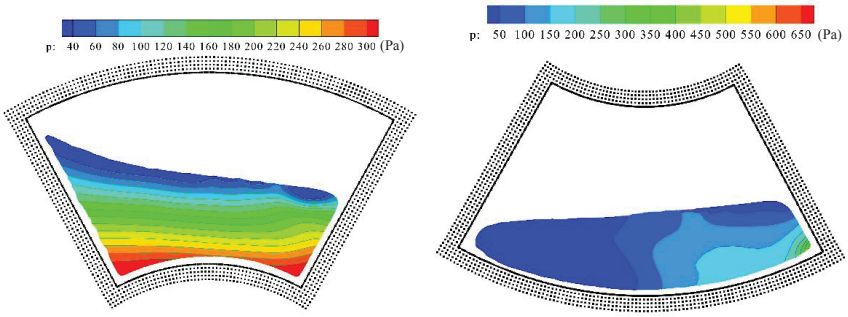

(a) $\alpha = \pi/2$ (b) $\alpha = 3\pi/2$

Figure 11: Pressure distribution for $\alpha = \pi/2$ and $\alpha = 3\pi/2$ at $\omega = 2.5$ rad/s

by centrifugal force analyzed before. In Fig.10a, the particles in the left zone are forced moving by the left side wall, thus, the maximum pressure appear in the left zone. Comparing Fig.10b with Fig.11b, it can be observed that there are great differences in the pressure distribution between two results. For the lower angular velocity, the fluid flows to the bottom of the barrel mainly under the effect of gravity, thus the maximum pressure appears in the bottom; for the higher one, the right side wall exerts a lot of thrust on the fluid, thus the maximum pressure appears in the lower right corner.

7 Conclusion

In this paper, a free surface flow with a forced revolving moving boundary model for screw extrusion is simulated by the ISPH methods. A set of organic glass forced revolving moving boundary fluid experimental device is manufactured. The free surfaces of computation are in good agreement with experimental data. When at a lower angular velocity ($\omega = 0.5$ rad/s), the free surface calculated by ISPH is almost a horizontal line; at higher speeds ($\omega = 2.5$ rad/s), the free surface shows to be a curve under stronger shear by the tank and barrel. With the increase of the speed, the average velocity of fluid increases, and the effect of centrifugal force will be revealed, on the other hand, for a low speed ($\omega \leq 1.5$ rad/s), the effect of centrifugal force can be negligible. The analysis of pressure distribution also discovers that with the increase of the speed, the maximum pressure increase, because the particles subject more shear from the barrel, more thrust from the side wall and more centrifugal All the discussions above show that the ISPH method is effective in simulating the partially filled flow problem for screw extrusion. This lays a foundation for future research on more complex flows in screw extrusion.

Acknowledgement: This work was supported by the National Natural Science Foundation of China (Grant No. 50863003) and the Research Foundation of Shangrao Normal University (Grant No. 0708).

References

Avila, R.; Atluri, S. N. (2009): Numerical Solution of Non-steady Flows, Around surfaces in spatially and temporally arbitrary motions, by using the MLPG method. *CMES: Computer Modeling in Engineering & Sciences*, vol. 54, no. 1, pp. 15-64.

Avila, R.; Han, Z.; Atluri, S. N. (2011): A novel MLPG-finite-volume mixed method for analyzing Stokesian flows & study of a new vortex mixing flow. *CMES: Computer Modeling in Engineering & Sciences*, vol. 71, no. 4, pp. 363-396.

Barrera, M. A.; Vega, J. F.; Martínez, S. J. (2008): Three-dimensional modelling of flow curves in co-rotating twin-screw extruder elements. *Journal of materials processing technology*, vol. 197, no. 1, pp. 221–224.

Belytschko, T.; Krongauz, Y.; Organ, D.; Fleming, M.; Krysl, P. (1996): Meshless methods: An overview and recent developments. *Comput. Methods Appl. Mech. Engrg.*, vol. 139, no. 1-4, pp. 3-47.

Campbell, J. C.; Vignjevic, R.; Patel, M.; Milisavljevic, S. (2009): Simulation of Water Loading On Deformable Structures Using SPH. *CMES: Computer Modeling in Engineering & Sciences*, vol. 49, no. 1, pp. 1-21.

Chorin, A. J. (1968): Numerical solution of the Navier Stokes equations. *Math. Comp.*, vol. 22, pp. 745-762.

Colagrossi, A.; Landrini, M. (2003): Numerical simulation of interfacial flows by smoothed particle hydrodynamics. *Journal of Computational Physics*, vol. 191, no. 2, pp. 448-475.

Cummins, S. J.; Rudman, M. (1999): An SPH projection method. *Journal of Computational Physics*, vol. 152, no. 2, pp. 584-607.

Delorme, L.; Colagrossi, A.; Souto-Iglesias, A.; Zamora-Rodriguez, R., Botia-Vera, E. (2009): A set of canonical problems in sloshing, Part I: Pressure field in forced roll comparison. *Ocean Engineering*, vol. 36, no. 2, pp. 168-178.

Gingold, R. A.; Monaghan, J. J. (1977): Smoothed particle hydrodynamics: theory and application to non-spherical stars. *Mon. Not. R. Astron. Soc*, vol. 181, no. 2, pp. 375-389.

Graaf, R. A. D.; Woldringh, D. J.; Janssen, L.P.B.M. (1999): Material Distribution in the Partially Filled Zone of a Twin-Screw Extruder. *Advances in Polymer Technology*, vol. 18, no. 4, pp. 295–302.

Hu, X. Y.; Adams, N. A. (2009): A constant-density approach for incompressible

multi-phase SPH. *Journal of Computational Physics*, vol. 228, no. 6, pp. 2082-2091.

Hughes, J. P.; GRAHAM, D. I. (2010): Comparison of incompressible and weakly-compressible SPH models for free-surface water flows. *Journal of Hydraulic Research*, vol. 48, Extra Issue, pp. 105-117.

Kakuda, K.; Nagashima, T.; Hayashi, Y.; Obara, S.; Toyotani, J.; Katsurada, N.; Matsuda, S. (2012): Particle-based fluid flow simulations on GPGPU Using CUDA. *CMES: Computer Modeling in Engineering & Sciences*, vol. 88, no. 1, pp. 17-28.

Kakuda, K.; Obara, S.; Toyotani, J.; Meguro, M.; Furuichi, M. (2012): Fluid flow simulation using particle method and its physics-based computer graphics. *CMES: Computer Modeling in Engineering & Sciences*, vol. 83, no. 1, pp. 57-72.

Khalifeh, A.; Clermont, J. R. (2005): Numerical simulations of non-isothermal three-dimensional flows in an extruder by a finite-volume method. *J. Non-Newtonian Fluid Mech.*, vol. 126, no. 1, pp. 7–22.

Kosec, G; Sarler, B. (2008): Local RBF collocation method for Darcy flow. *CMES: Computer Modeling in Engineering & Sciences*, vol. 25, no. 3, pp. 197-207.

Lee, E. S.; Moulinec, C.; Xu, R.; Violeaua, D.; Laurencec, D.; Stansby, P. (2008): Comparisons of weakly compressible and truly incompressible algorithms for the SPH mesh free particle method. *Journal of Computational Physics*, vol. 227, no.18, pp. 8417-8436.

Lucy, L. B. (1977): A numerical approach to the testing of the fission hypothesis. *Astrophys. J.*, vol. 82, no. 2, pp. 1013-1024.

Monaghan J. J. (2006): Smoothed particle hydrodynamic simulations of shear flow. *Monthly Notices of the Royal Astronomical Society*, vol. 365, no. 1, pp. 199-213.

Monaghan, J. J. (2000): SPH without a tensile instability. *Journal of Computational Physics*, vol. 159, no. 2, pp. 290-311.

Monaghan, J. J.; Kos, A. (1999): A solitary wave on a Cretan beach. *J. Waterways, Ports, Coastal and Ocean Eng*, vol. 125, no. 3, pp. 145-154.

Monaghan, J. J. (1994): Simulating free surface flows with SPH. *Journal of Computational Physics,* vol. 110, no. 2 pp. 399-406.

Monaghan, J. J. (1992): Smoothed Particle Hydrodynamics. *Annu. Rev. Astron. Astrophys,* vol. 30, pp. 543-74.

Morris, J. P.; For, J. P.; Yi, Zhu. (1997): Modeling low Reynolds number incompressible flows using SPH. *Journal of Computational Physics*, vol. 136, no. 1. pp. 214-226.

Moulinec, C; Issa, R; Marongiu, J.C; Violeau, D. (2008): Parallel 3-D SPH Simulations. *CMES: Computer Modeling in Engineering & Sciences*, vol.25, no.3, pp.133-147.

Nguyen, V. P.; Rabczuk, T.; Bordas, S.; Duflot, M. (2008): Meshless methods: A review and computer implementation aspects. *Mathematics and Computers in Simulation*, vol. 79, no. 3, pp. 763-813.

Prakash, M.; Cleary, P.; Grandfield, J. (2009): Modelling of metal flow and oxidation during furnace emptying using smoothed particle hydrodynamics. *Journal of materials processing technology*, vol. 209, no. 7, pp. 3396–3407.

Rafiee, A.; Cummins, S.; Rudman, M; Thiagarajan, K. (2012): Comparative study on the accuracy and stability of SPH schemes in simulating energetic free-surface flows. *European Journal of Mechanics B/Fluids*, vol. 36, pp. 1-16.

Shao, S. D. (2012): Incompressible smoothed particle hydrodynamics simulation of multifluid flows. *Int. J. Numer. Meth. Fluids*, vol. 69, no. 11, pp. 1715-1735.

Shao, S.; Lo, E.Y.M. (2003): Incompressible SPH method for simulating Newtonian and non-Newtonian flows with a free surface. *Adv. Water Resour.*, vol. 26, no.7, pp. 787-800.

Van Der Vorst, H. A. (1992): Bi-CGSTAB: A fast and smoothly converging variant of Bi-CG for the solution of non-symmetric linear systems. *S. J. Sci. Stat. Comput.*, vol. 13, no. 2, pp. 631-644.

Xu, R.; Stansby, P.; Laurence, D. (2009): Accuracy and stability in incompressible SPH (ISPH) based on the projection method and a new approach. *Journal of Computational Physics*, vol. 228, no. 18. pp. 6703-6725.

Zhu, X. Z.; Yuan, H. Q.; Wang, W. Q. (2009): Numerical simulation of flow characteristics in new co-rotating triangle arrayed triple screw extruders. *Journal of Materials Processing Technology*, vol. 209, no. 7, pp. 3289–3299.